

Journal of Materials Chemistry C

Accepted Manuscript



This is an *Accepted Manuscript*, which has been through the Royal Society of Chemistry peer review process and has been accepted for publication.

Accepted Manuscripts are published online shortly after acceptance, before technical editing, formatting and proof reading. Using this free service, authors can make their results available to the community, in citable form, before we publish the edited article. We will replace this *Accepted Manuscript* with the edited and formatted *Advance Article* as soon as it is available.

You can find more information about *Accepted Manuscripts* in the [Information for Authors](#).

Please note that technical editing may introduce minor changes to the text and/or graphics, which may alter content. The journal's standard [Terms & Conditions](#) and the [Ethical guidelines](#) still apply. In no event shall the Royal Society of Chemistry be held responsible for any errors or omissions in this *Accepted Manuscript* or any consequences arising from the use of any information it contains.



Journal Name

ARTICLE

N-heteroheptacenequinone and N-heterononacenequinone: synthesis, physical properties, crystal structures and photoelectrochemical behaviors

Received 00th January 20xx,
Accepted 00th January 20xx

DOI: 10.1039/x0xx00000x

www.rsc.org/

Junbo Li^{a,b}, Jianwei Miao^c, Guankui Long^a, Jing Zhang^a, Yongxin Li^d, Rakesh Ganguly^d, Yang Zhao^a, Yi Liu^e, Bin Liu^{c*}, Qichun Zhang^{a,d*}

N-heteroquinones with both quinone and pyrazine as electron-withdrawing moieties, can be potential candidates of n-type organic semiconductor materials. Here, two novel soluble N-heteroquinones: 5,9,14,18-tetra-(triisopropylsilyl)ethynyl-6,8,15,17-tetraazaheptacene-7,16-dione (**TAHD**) and 6,10,17,21-tetra-((triisopropylsilyl)ethynyl)-7,9,18,20-tetraazanonacene-8,19-dione (**TAND**) with different length have been synthesized and their structures were fully characterized by ¹H NMR, ¹³C NMR, HRMS and single crystal analysis. Our studies showed that the shorter **TAHD** molecules are planar in solid state without intermolecular π - π stacking and the main force to stabilize the packing is the C-H- π interaction between (triisopropylsilyl)ethynyl (TIPS) groups and the backbones. Differently, the larger **TAND** molecules show slightly twisted structures with the anthracene units bent down and up on the two sites and the dihedral angle between quinone unit and anthracene unit is 6.7°. Meanwhile, **TAND** molecules adopt face-to-face two-dimension (2D) brickwork arrangement, and the distances between π planes are 3.63 and 3.38 nm, respectively, suggesting the existence of π - π interactions. The visible-light-driven photoelectrochemical behaviors showed that both **TAHD** and **TAND** are n-type semiconductors. However, **TAHD** shows unstable photovoltage response and lower photocurrent due to the absence of π - π interaction while **TAND** shows stable photovoltage response and relative higher photocurrent. Our results suggested that the length of the linear N-heteroquinones could have large effects on their physical properties, crystal packing and photoelectrochemical behaviors.

Introduction

N-heteroacenes (azaacenes),¹ in which sp² N atoms replace the CH groups in the backbones of acenes,² have emerged as promising organic semiconductor materials. Current researches have already demonstrated that the position, number and valence of N atoms in the frameworks of azaacenes have strong effects on the properties of as-resulted azaacenes.³ For example, N-heteropentacenes have been investigated to show p-type,⁴ ambipolar⁵ and n-type⁶ charge-transporting properties according to the variation of the number and position of N atoms. An electron mobility as high as 3.3 cm² V⁻¹ S⁻¹ has been achieved in organic field effect

transistors (OFETs) based on 5,7,12,14-tetraaza-6,13-bis(triisopropylsilyl)ethynyl)pentacene.⁶ Beside their applications in OFETs, N-heteroacenes have also been employed as active materials in other organic electronic devices such as organic light-emitting diodes (OLEDs),⁷ phototransistors,⁸ solar cells,⁹ photoelectrochemical cells,¹⁰ and memories¹¹. Also, these materials have great potential for ion detection.¹² Although N-heteroacenes have a lot of attractive properties, larger azaacenes (n > 6) become extremely unstable and insoluble.¹³ New strategies to address these problems and achieve larger azaacenes are highly desirable.

Considering the poor stability of azaacenes, introducing quinone units into azacene systems could be another good strategy to approach larger stable n-type organic semiconductor materials, because (1) quinone is a good electron-withdrawing group; (2) quinone will reduce the degree of π -conjugation; and (3) quinone is an air-stable unit. In fact, N-heteropentacenequinones have been known for decades,¹⁴ however, their semiconductor properties have never been explored until Miao's group demonstrated that N-heteropentacenequinones are n-type organic semiconductor materials with electron mobilities as high as 0.05-0.12 cm² V⁻¹ s⁻¹.¹⁵ Generally, larger N-heteroquinones should be a promising class of materials for either the preparation of N-

^aSchool of Materials Science and Engineering, Nanyang Technological University, Singapore 639798, Singapore. E-mail: gczhong@ntu.edu.sg; Tel: (+65) 6790 4705.

^bSchool of Chemistry and Environmental Engineering, Wuhan Institute of Technology, Wuhan 430074, China.

^cSchool of Chemistry and Biomedical Engineering, Nanyang Technological University, Singapore 637459, Singapore. E-mail: liubin@ntu.edu.sg.

^dDivision of Chemistry and Biological Chemistry, School of Physical and Mathematical Sciences, Nanyang Technological University, Singapore 637371, Singapore.

^eThe Molecular Foundry, Lawrence Berkeley National Laboratory, Berkeley, California, 94720, United States.

Electronic Supplementary Information (ESI) available: Crystallographic data for **TAHD** and **TAND**, all ¹H NMR, ¹³C NMR, HR-MS, FTIR spectra and TGA curves. See DOI: 10.1039/x0xx00000x

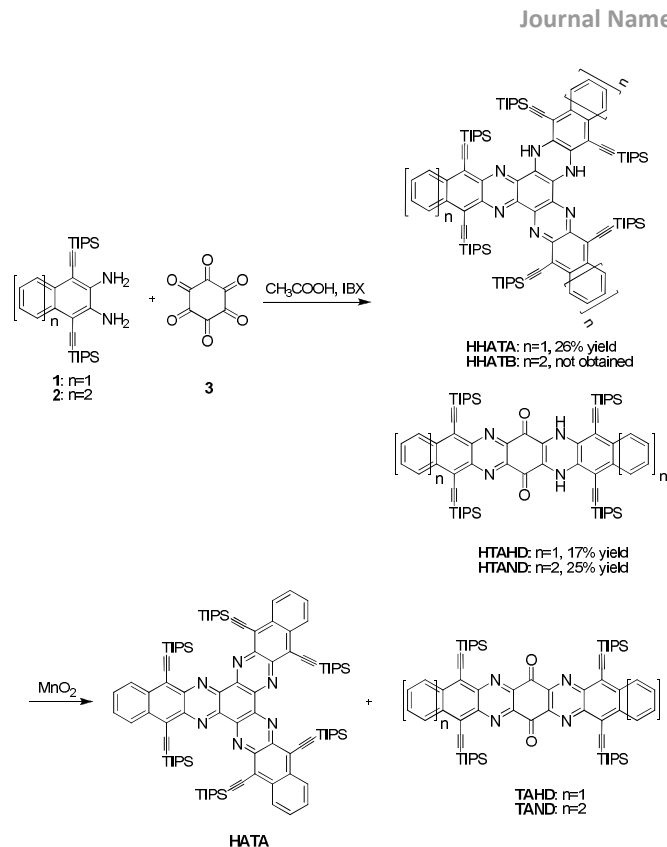
ARTICLE

heteroacenes¹⁶ or the fabrication of high performance n-type semiconductor devices. However, the preparation and physical properties of larger N-heteroquinones ($n > 5$) are rarely explored. Until very recently, our group developed an effective one-step condensation reaction to successfully construct 6,10,17,21-tetra-((triisopropylsilyl)ethynyl)-5,7,9,11,16,18,20,22-octaazanonacene-8,19-dione.¹⁷ The as-prepared octaazanonacenequinone showed an electron mobility up to $0.2 \text{ cm}^2 \text{ V}^{-1} \text{ s}^{-1}$.¹⁷ Continuing our research efforts to further understand the structure-property relationships of N-heteroquinones, we prepared two novel TIPS-containing N-heteroquinones (5,9,14,18-tetra-((triisopropylsilyl)ethynyl)-6,8,15,17-tetraazaheptacene-7,16-dione (**TAHD**) and 6,10,17,21-tetra-((triisopropylsilyl)ethynyl)-7,9,18,20-tetraazanonacene-8,19-dione (**TAND**). Their structures and physical properties have been carefully investigated. Moreover, photoelectrochemical cells with as-prepared N-heteroquinones (**TAHD** and **TAND**) as active materials have been fabricated and investigated because this type of cells has been widely used to study the visible-light-driven photoelectrical behaviors and the character of charge carriers of inorganic semiconductors and organic ones (rare case).¹⁸ Our results show that both **TAHD** and **TAND** display visible-light-driven photoelectrical behaviors with n-type character.

Results and discussion

Synthesis of **TAHD** and **TAND**

Scheme 1 shows the synthesis of **TAHD** and **TAND**. 1,4-bis((triisopropylsilyl)ethynyl)naphthalene-2,3-diamine (**1**)¹⁹ and 1,4-bis((triisopropylsilyl)ethynyl)anthracene-2,3-diamine (**2**)²⁰ were synthesized by six steps according to the reported procedures, respectively. Both 5,8,13,16,21,24-hex-(triisopropylsilyl)ethynyl)-6,23-dihydro-6,7,14,15,22,23-hexazatrianthrylene (**HHATA**) and 5,9,14,18-tetra-((triisopropylsilyl)ethynyl)-6,17-dihydro-6,8,15,17-tetraazaheptacene-7,16-dione (**HTAHD**) were obtained in one step with yields of 26% (for **HHATA**) and 17% (for **HTAHD**), through the condensation between **1** and hexaketocyclohexane octahydrate (**3**) in acetic acid. Further oxidation of **HHATA** and **HTAHD** with MnO_2 could give **HATA** and **TAHD** in high yield (92% each). Surprisingly, under the same condensation condition, when the condensation between **2** and hexaketocyclohexane octahydrate (**3**) was performed, no triply fused 7,10,17,20,27,30-hex-(triisopropylsilyl)ethynyl)-8,29-dihydro-8,9,18,19,28,29-hexazatribenz[b]anthrylene (**HHATB**) was observed and the main product was the linearly fused compound 6,10,17,21-tetra-((triisopropylsilyl)ethynyl)-7,20-dihydro-7,9,18,20-tetraazanonacene-8,19-dione (**HTAND**), which followed our previously-investigated result (the condensation between 1,4-bis((triisopropylsilyl)ethynyl)phenazine-2,3-diamine with hexaketocyclohexane octahydrate (**3**)).¹⁷ **HTAND** can be further oxidized by MnO_2 to give **TAND** with a yield of 85%.



Scheme 1 The synthesis of **TAHD** and **TAND**.

Compounds **TAHD** and **TAND** were fully characterized by ^1H NMR, ^{13}C NMR, HRMS and single crystal analysis.

Structure analysis of **TAHD** and **TAND**

Single crystals of **TAHD** and **TAND** suitable for single crystal X-ray analysis were obtained through slow evaporation of the mixed solvents of $\text{CH}_2\text{Cl}_2/\text{CH}_3\text{OH}$ ($v/v = 5:1$ for **TAHD**) and $\text{CH}_2\text{Cl}_2/\text{CH}_3\text{CN}$ ($v/v = 5:1$ for **TAND**). Figure 1 shows the molecular structures and molecular packing patterns of **TAHD** and **TAND**. Obviously, **TAHD** has a planar structure in the solid state (Figure 1a) and the steric effect of four TIPS groups strongly hinders the π - π stacking between the neighboring **TAHD** molecules (Figure 1b). The main force to stabilize the packing of **TAHD** molecules is the C-H- π interaction between TIPS groups and the N-heteroquinone core. This result is similar to that of N,N-dihydro-tetraazaheptacene reported by Bunz et al.²¹ Interestingly, when the length of acene's backbone was extended from N-heteroheptacenequinone (**TAHD**) to N-heterononacenequinone (**TAND**), several differences are observed in molecular structures and packing patterns: (1) **TAND** displays a slightly twisted structure with anthracene unit on one side of quinone bending up and the other anthracene unit on another side bending down, with dihedral angle of 6.7° (Figure 1c), in contrast to the planar structure of **TAHD**. This bending in **TAND** might reduce the steric hindrance induced by four TIPS groups and favor the packing of N-heteroquinone backbones.¹⁷ (2) **TAND** molecules adopt a face-to-face two-dimension (2D) brickwork arrangement with unequal overlapping areas. The interplanar distances are 3.63 and 3.38 nm (Figure 1d), respectively,

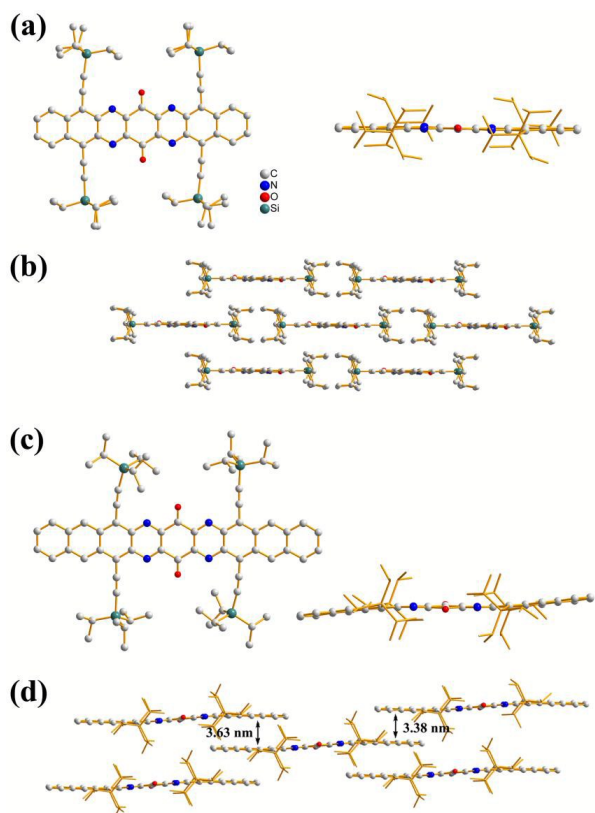


Fig. 1 (a) Single crystal structures of **TAHD** (left: top view; right: side view). (b) Packing structures of **TAHD**. (c) Single crystal structures of **TAND** (left: top view; right: side view). (d) Packing structures of **TAND**.

suggesting the existence of π - π stacking. In **TAHD**, intermolecular stacking is stabilized through C-H- π interaction.

Theoretical calculations

The molecular geometries of compounds **HTAHD**, **TAHD**, **HTAND** and **TAND** were optimized by using density functional theory (DFT) at the B3LYP/6-31G* level,²² and the frequency analysis was followed to assure that the optimized structures were stable states. As shown in Figure 2, the highest occupied molecular orbital (HOMO) of **HTAHD** and **HTAND** is mainly localized on the dihydropyrazine unit and the naphthalene or anthracene unit, while the lowest unoccupied molecular orbital (LUMO) is mainly localized on the quinone unit, which indicates the existence of strong intramolecular charge transfer (ICT) in **HTAHD** and **HTAND**. This is caused by the strong electron-donating ability of the lone pairs on nitrogen atoms in dihydropyrazine units, and the calculated HOMO and LUMO orbital energies of **HTAHD** and **HTAND** are very close, which is in accordance with the experimental results (Table 1). The HOMO orbital of **TAHD** and **TAND** is mainly localized on the two naphthalene or anthracene units, while LUMO orbital is localized on the whole backbone. Meanwhile, the calculated results showed that both HOMO and LUMO orbital energies were decreased with the extension of backbone from **TAHD** to **TAND**, while the energy decrease of HOMO is larger than that of LUMO. The calculated results of HOMO, LUMO and

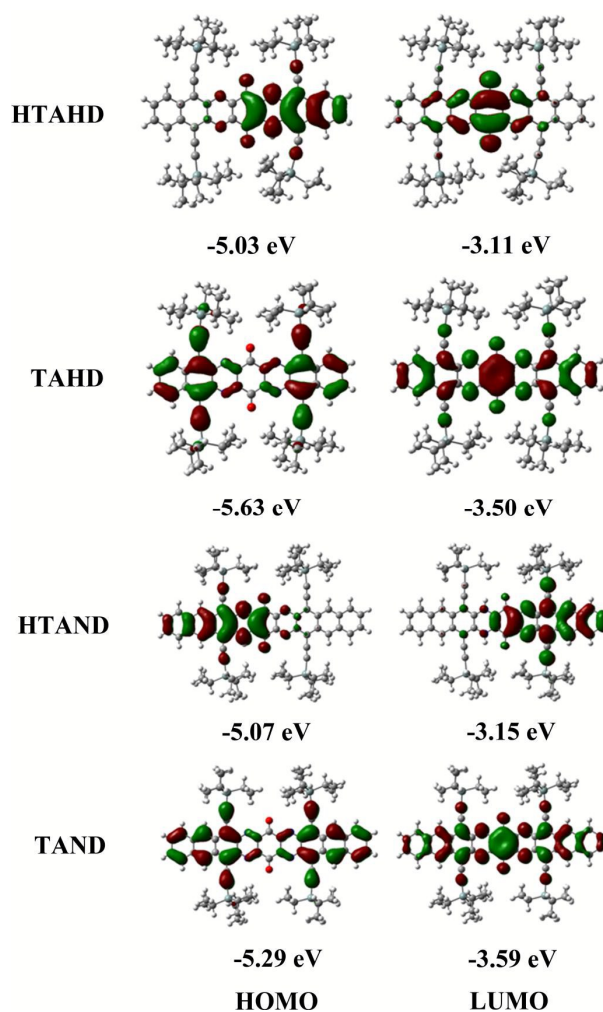


Fig. 2 Wave functions for the HOMO and LUMO of compounds **HTAHD**, **TAHD**, **HTAND** and **TAND**.

bandgaps are summarized in Table 1.

Optical and electrochemical properties

Figure 3 shows UV-vis spectra of compounds **HTAHD**, **TAHD**, **HTAND** and **TAND** in CH_2Cl_2 . The solution of **HTAHD** (1×10^{-5} M) shows a longest-wavelength absorption at 680 nm due to the existence of ICT from electron donor (NH) to electron acceptor (pyrazine ring). After oxidation, the longest-wavelength absorption peak was blue-shifted to 601 nm, indicating the decrease of ICT. Accordingly, the color of solutions was changed from purple (**HTAHD**, 1×10^{-5} M, CH_2Cl_2 , Figure 3) to light green (**TAHD**, 1×10^{-5} M, CH_2Cl_2 , Figure 3). When the backbone was extended from **TAHD** to **TAND**, a red-shifted absorption was observed. The precursor **HTAND** shows a broad absorption in the range of 470-860 nm with a maximum absorption peak (longest one) at 790 nm, which is larger than that of **HTAHD**. This can be explained by the extended π conjugation, which can be further confirmed by the wave functions of HOMO and LUMO of **HTAHD** and **HTAND** (Figure 2). After oxidation, the longest absorption peak of **TAND** was blue-shifted to 740 nm. The color of solution was also changed from blue (**HTAND**, 1×10^{-5} M, CH_2Cl_2 , Figure 3) to

Table 1 Experimental and calculated HOMO-LUMO gaps of compounds **HTAHD**, **TAHD**, **HTAND** and **TAND**.

Comp	$E_{\text{onset}}^{\text{red}}$ (V) ^a	$E_{\text{onset}}^{\text{ox}}$ (V) ^a	E_{gap} (eV) ^b	LUMO (eV) ^c	HOMO (eV) ^d	$E_{\text{gap}}/\lambda_{\text{onset}}$ [(eV) ^e /nm]	LUMO (eV) ^f	HOMO (eV) ^f	E_{gap} (eV) ^f
HTAHD	-1.04	0.34	1.38	-3.76	-5.14	1.50/823	-3.11	-5.03	1.92
TAHD	-0.71	1.12	1.83	-4.09	-5.92	1.84/673	-3.50	-5.63	2.13
HTAND	-1.02	0.34	1.36	-3.78	-5.14	1.43/870	-3.15	-5.07	1.92
TAND	-0.63	0.82	1.45	-4.17	-5.62	1.48/836	-3.59	-5.29	1.71

[a] Obtained from cyclic voltammograms in CH_2Cl_2 . [b] $E_{\text{gap}} = E_{\text{onset}}^{\text{ox}} - E_{\text{onset}}^{\text{red}}$. [c] Calculated according to the formula $E_{\text{LUMO}} = -4.8 \text{ eV} - E_{\text{red}}$. [d] Calculated from $E_{\text{HOMO}} = E_{\text{LUMO}} - E_{\text{gap}}$. [e] Optical band gap, $E_{\text{gap}} = 1240/\lambda_{\text{onset}}$. [f] Obtained from theoretical calculations.

yellow (**TAND**, $1 \times 10^{-5} \text{ M}$, CH_2Cl_2 , Figure 3).

The electrochemical properties of compounds **HTAHD**, **TAHD**, **HTAND** and **TAND** were shown in Figure 4 and the data were summarized in Table 1. The **HTAHD** shows two irreversible oxidation peaks and four irreversible reduction peaks with the onset oxidation and onset reduction potentials at 0.34 and -1.04 V, respectively (all the potentials are illustrated versus Fc^+/Fc unless specified). The HOMO and LUMO orbital energies of **HTAHD** are estimated to be -5.14 and -3.76 eV, respectively, according to the equation $E_{\text{LUMO}} = -4.8 \text{ eV} - E_{\text{red}}$ and $E_{\text{HOMO}} = E_{\text{LUMO}} - E_{\text{gap}}$.²³ Interestingly, the onset oxidation and reduction potentials of the longer **HTAND** are located at 0.34 and -1.02 V ($E_{\text{HOMO}} = -5.14 \text{ eV}$, $E_{\text{LUMO}} = -3.78 \text{ eV}$), which were nearly the same as that of **HTAHD**, indicating that the extension of acene's backbone in *N,N*-dihydroetraazaacenequinones has little effect on the HOMO and LUMO energies, which is further supported by theoretical calculations (Table 1).

The **TAHD** shows one irreversible oxidation peaks and five reduction peaks (two reversible reduction peaks and three irreversible reduction peaks). The onset oxidation and reduction potentials were measured as 1.12 and -0.71 V, corresponding to calculated HOMO and LUMO energies of

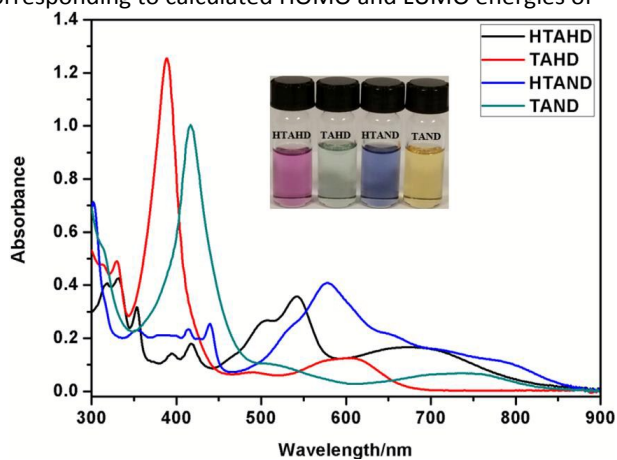


Fig. 3 The UV-vis spectra of compounds **HTAHD**, **TAHD**, **HTAND** and **TAND** in CH_2Cl_2 ($1 \times 10^{-5} \text{ M}$). The inset shows the solution colors of compounds **HTAHD**, **TAHD**, **HTAND** and **TAND**.

-5.92 and -4.09 eV, respectively. Obviously, the oxidation of dihydropyrazine to pyrazine ring largely decreases the HOMO and LUMO energies. As to the longer **TAND**, the HOMO and LUMO energies were also decreased from -5.14 (HOMO) and -3.78 eV (LUMO) (for **HTAND**) to -4.17 and -5.62 eV (for **TAND**), respectively. Actually, the **TAND** shows a higher HOMO and lower LUMO compared with **TAHD**. Meanwhile, the increase of HOMO energy is larger than the decrease of LUMO energy from **TAHD** to **TAND**, which indicated that the extending of *N*-heteroquinone's backbones has more effect on the energy level of HOMO than that of LUMO, which induced the decrease of bandgap of longer *N*-heteroquinones.

The surface morphologies of thin films for both compounds (prepared through spinning coating) have been investigated using atomic force microscopy (AFM). The morphological features of **TAHD** and **TAND** were different from each other (Figure S5). For **TAHD** molecule, thin film displayed smooth and continues morphology, however, the molecular interplane distance was much larger than Van der Waals' force, which leads to very poor π - π overlap. Thus, no mobility was observed. For longer **TAND** molecule with π - π stacking, there were obvious grain boundaries in the thin film, which restricts the effective charge transport. So far, we still couldn't obtain any charge transport for this film. The further effort to try other fabrication conditions to prepare high-quality film is still on the way.

Photoelectrochemical behaviors

Figure 5a shows the photovoltage (illuminated open-circuit potential) responses of **TAHD**. The negative photovoltage responses suggest that **TAHD** is an *n*-type semiconductor material. However, this material showed non-recoverable photovoltage responses, as its open-circuit potential (V_{oc}) changed constantly during the measurement, which might be

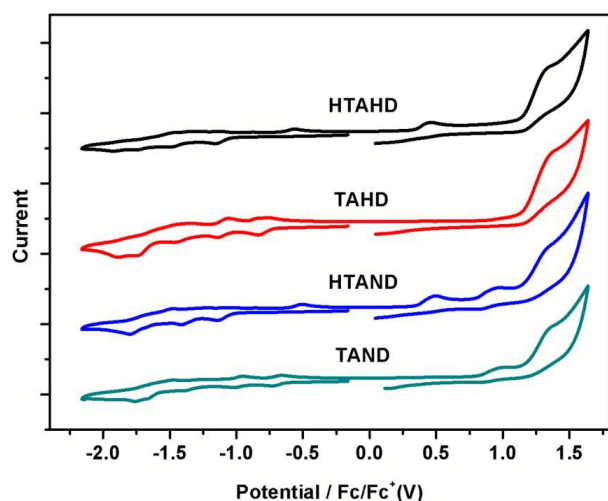


Fig. 4 Cyclic voltammetry curves of compounds **HTAHD**, **TAHD**, **HTAND** and **TAND** in CH_2Cl_2 solution containing 0.1 M tetrabutylammonium hexafluorophosphate (TBAF) electrolyte. Scanning rate: 100 mV/s.

caused by the poor conductivity of **TAHD** due to the absence of intermolecular π - π stacking in solid state. Figure 5b shows the photocurrent profile of **TAHD**/FTO electrode recorded under zero-bias (two-electrode, short-circuit) condition. The repeatable cathodic photocurrent of $\sim 12 \text{ nA/cm}^2$ suggests that **TAHD** is an n-type semiconductor, which is consistent with the result observed in photovoltage measurement. To further investigate the conductivity type and flat-band potential of **TAHD**, Mott-Schottky measurement was performed in 0.5 M Na_2SO_4 aqueous solution. As shown in Figure S7, the positive slope of the linear region on the plot indicates the n-type behavior of **TAHD**, which is again consistent with the results obtained from the previous photoelectrochemical measurements. The flat-band potential of **TAHD** estimated from the plot was about 0.083 V vs. RHE. Larger tetraazanonacenequinone (**TAND**) shows stronger intermolecular π - π stacking in solid state, which may enhance the photoelectrochemical responses and device stability. Figure 5c shows the photovoltage (illuminated open-circuit potential) response of **TAND**. The negative photovoltage responses suggest **TAND** is also an n-type semiconductor material. The photovoltage response of **TAND** is more stable compared with that of tetraazaheptacenequinone (**TAHD**), as there was no obvious shift in open-circuit potential throughout the test. Figure 5d shows the photocurrent profile of **TAND**/FTO. The highly repeatable anodic photocurrent with a magnitude of $\sim 23 \text{ nA/cm}^2$, which is higher and more stable than that of **TAHD**, affirmed its n-type conductive characteristic. The n-type behavior of **TAHD** was confirmed by Mott-Schottky measurement, as shown in Figure S8, and its flat-band potential was estimated around 0.193 V vs. RHE.

Experimental section

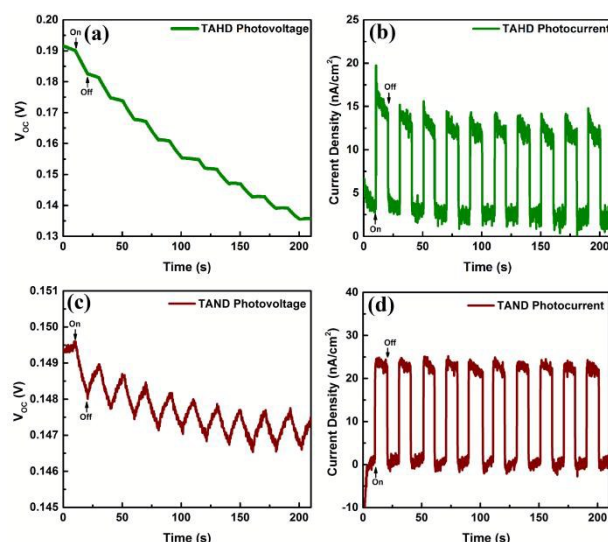


Fig. 5 The photoelectrochemical measurements of **TAHD** and **TAND** under chopped AM 1.5 G light illumination (a) Photovoltage (illuminated OCP) responses of **TAHD**/FTO electrode. (b) Zero-biased photocurrent responses of **TAHD**/FTO electrode. (c) Photovoltage (illuminated OCP) responses of **TAND**/FTO electrode. (d) Zero-biased photocurrent responses of **TAND**/FTO electrode.

General Information

The chemical reagents were purchased from Aldrich or TCI. Commercially available reagents were used without further purification except that THF was dried with standard procedure. Solution NMR spectra were taken on a Bruker Advance 300 spectrometer and the chemical shift values were given in ppm. The FTIR spectra (KBr pellets) were recorded on a PerkinElmer FTIR spectrophotometer in the range 400–4000 cm^{-1} . UV-Vis spectrum was recorded using a Shimadzu UV-2501 spectrometer. Electrochemistry was carried out with a CHI 600C, employing glassy carbon (diameter: 1.6 mm; area 0.02 cm^2), platinum wire and platinum wire as working electrode, counter electrode, and reference electrode, respectively. Tetrabutylammonium hexafluorophosphate (0.1 M) in methylene chloride was used as an electrolyte at room temperature under Argon. The potential was externally calibrated against the ferrocene/ferrocenium couple. HR-MS (ESI) spectra were recorded on a Waters Q-ToFpremierTM mass spectrometer. Thermogravimetric analysis (TGA) was carried out on a TA Instrument Q500 Thermogravimetric Analyzer at a heating rate of 10 $^\circ\text{C}/\text{min}$ up to 800 $^\circ\text{C}$.

Syntheses

The synthesis of 5,8,13,16,21,24-hex(triisopropylsilyl)ethynyl)-6,23-dihydro-6,7,14,15,22,23-hexazatrianthrylene (HHATA) and 5,9,14,18-tetra(triisopropylsilyl)ethynyl)-6,17-dihydro-6,8,15,17-tetraazaheptacene-7,16-dione (HTAHD):

The mixture of 1,4-bis((triisopropylsilyl)ethynyl)naphthalene-2,3-diamine (1 g, 1.93 mmol), hexaketocyclohexane octahydrate (273 mg, 0.88 mmol) and catalytic amount IBX in acetic acid (80 mL) was refluxed for 48 h under argon. The mixture was poured into water, then extracted with methylene chloride (200 mL \times 3), the combined organic solvent was dried with Na₂SO₄. The solvent was removed in *vacuo*. The solids were further purified by chromatography on silica gel using hexanes/CH₂Cl₂ (v/v = 5:1) solvent mixture. Compound **HTAHD** (170 mg, 17% yield) and **HHATA** (270 mg, 26% yield) were obtained, respectively.

HTAHD: IR (KBr, cm⁻¹): ν 3355, 2944, 2860, 2133, 1654, 1623, 1585, 1484, 1470, 1428, 1388, 1368, 1332, 1264, 1221, 1155, 1033, 1015, 994, 876, 710, 679, 654, 568, 512. ¹H NMR (CDCl₃, 300 MHz) δ : 8.72 (dd, 2H), 7.73-7.78 (m, 4H), 7.27-7.31 (m, 4H), 1.26-1.38 (m, 84H). ¹³C NMR (CDCl₃, 75 MHz) δ 171.1, 144.2, 140.4, 135.8, 133.7, 130.9, 130.8, 129.4, 128.1, 127.1, 125.5, 123.1, 109.9, 108.1, 103.6, 101.4, 98.5, 19.1, 19.0, 11.7, 11.5. HRMS (ESI-TOF) m/z: [M+H]⁺ calcd 1135.6532, found 1135.6476.

HHATA: IR (KBr, cm⁻¹): ν 3376, 3062, 2942, 2864, 2127, 1623, 1558, 1507, 1473, 1428, 1381, 1261, 1206, 1155, 1076, 990, 881, 765, 734, 676, 577, 508. ¹H NMR (CDCl₃, 300 MHz) δ : 8.75 (dd, 4H), 7.86-7.90 (m, 4H), 7.69-7.73 (m, 4H), 7.28-7.30 (m, 2H), 1.15-1.33 (m, 126H). ¹³C NMR (CDCl₃, 75 MHz) δ : 141.5, 139.3, 138.6, 136.7, 135.5, 134.7, 134.1, 131.3, 128.5, 127.8, 127.4, 127.2, 126.8, 126.2, 125.0, 121.8, 118.0, 109.0, 108.0, 104.0, 103.4, 102.8, 101.0, 100.4, 19.4, 11.7. HRMS (ESI-TOF) m/z: [M+H]⁺ calcd 1617.9833, found 1617.9896.

The synthesis of 5,9,14,18-tetra-(triisopropylsilyl)ethynyl)-6,8,15,17-tetraazaheptacene-7,16-dione (TAHD):

HTAHD (150 mg) and MnO₂ (150 mg) were added into the flask with 20 mL CH₂Cl₂, and the mixture was stirred at RT for 1 h. The solution was evaporated and the solid was purified by chromatography on silica gel using hexanes/CH₂Cl₂ (v/v = 3:1) solvent mixture. Compound **TAHD** (138 mg, 92% yield) was obtained. IR (KBr, cm⁻¹): ν 3061, 3011, 2941, 2862, 2140, 1711, 1544, 1461, 1439, 1417, 1391, 1378, 1315, 1125, 1061, 1034, 1016, 994, 877, 767, 716, 679, 652, 571. ¹H NMR (CDCl₃, 300 MHz) δ : 8.81 (dd, 4H), 7.82 (dd, 4H), 1.34-1.41 (m, 84H). ¹³C NMR (CDCl₃, 75 MHz) δ 178.0, 144.7, 141.1, 136.8, 130.0, 128.1, 123.6, 111.3, 101.1, 19.0, 11.6. HRMS (ESI-TOF) m/z: [M+H]⁺ calcd 1133.6376, found 1133.6417.

The synthesis of 5,8,13,16,21,24-hex-(triisopropylsilyl)ethynyl)-6,7,14,15,22,23-hexazatrianthrylene (HATA):

The procedure is the same with the synthesis of **TAHD** (92% yield). **TAHD** was purified by chromatography on silica gel using hexanes/CH₂Cl₂ (v/v = 2:1) solvent mixture. IR (KBr, cm⁻¹): ν 3064, 2942, 2863, 2139, 1460, 1412, 1385, 1223, 1148, 995, 881, 825, 762, 736, 678, 664, 579. ¹H NMR (CDCl₃, 300 MHz) δ : 8.82 (dd, 6H), 7.76 (dd, 6H), 1.16-1.31 (m, 126H). ¹³C NMR (CDCl₃, 75 MHz) δ 143.6, 140.9, 135.8, 128.6, 128.0, 122.0,

109.6, 102.7, 19.1, 11.9. HRMS (ESI-TOF) m/z: [M+H]⁺ calcd 1615.9677, found 1615.9583.

The synthesis of 6,10,17,21-tetra-(triisopropylsilyl)ethynyl)-7,20-dihydro-7,9,18,20-tetraazanonacene-8,19-dione (HTAND):

The mixture of 1,4-bis((triisopropylsilyl)ethynyl)anthracene-2,3-diamine (1 g, 1.76 mmol), hexaketocyclohexane octahydrate (250 mg, 0.80 mmol) and catalytic amount IBX in acetic acid (80 mL) was refluxed for 48 h. The mixture was poured into water, then extracted with methylene chloride (200 mL \times 3). The combined organic solvent was dried with Na₂SO₄, then the solvent was evaporated in *vacuo*. The solids were further purified by chromatography on silica gel using hexanes/CH₂Cl₂ (v/v = 5:1) solvent mixture. Compound **HTAND** (247 mg, 25% yield) was obtained. IR (KBr, cm⁻¹): ν 3348, 3046, 2942, 2860, 2134, 1651, 1614, 1489, 1467, 1435, 1408, 1324, 1224, 1182, 1143, 1055, 995, 929, 880, 730, 676, 662, 574. ¹H NMR (CDCl₃, 300 MHz) δ : 9.38 (s, 2H), 8.27 (s, 2H), 8.08 (dd, 2H), 7.81 (dd, 2H), 7.79 (s, 2H), 7.59 (dd, 2H), 7.41 (dd, 2H), 1.27-1.42 (m, 84H). ¹³C NMR (CDCl₃, 75 MHz) δ 171.0, 144.1, 139.7, 133.7, 133.3, 132.7, 132.6, 130.0, 129.0, 128.6, 128.2, 127.8, 127.6, 126.3, 124.3, 123.6, 110.9, 106.6, 102.5, 102.2, 98.8, 19.1, 19.0, 11.8, 11.6. HRMS (ESI-TOF) m/z: [M+H]⁺ calcd 1235.6845, found 1235.6847.

The synthesis of 6,10,17,21-tetra-(triisopropylsilyl)ethynyl)-7,9,18,20-tetraazanonacene-8,19-dione (TAND):

The procedure is the same with the synthesis of **TAHD** (85% yield). IR (KBr, cm⁻¹): ν 3046, 2942, 2860, 2134, 1651, 1614, 1489, 1467, 1435, 1408, 1324, 1224, 1182, 1143, 1055, 995, 929, 880, 730, 676, 662, 574. ¹H NMR (CDCl₃, 300 MHz) δ : 9.49 (s, 4H), 8.11 (dd, 4H), 7.61 (dd, 4H), 1.38-1.44 (m, 84H). ¹³C NMR (CDCl₃, 75 MHz) δ 178.0, 144.6, 140.2, 134.0, 133.4, 128.9, 127.9, 124.2, 112.7, 102.1, 19.0, 11.7. HRMS (ESI-TOF) m/z: [M+H]⁺ calcd 1233.6689, found 1233.6643.

Single crystal growth and data collection

TAHD (5 mg) was dissolved with methylene chloride (5 mL) in a 10 mL glass bottle, and then, 1 mL of methanol was added into the solution. The bottle was sealed with parafilm, and the surface of parafilm was punched three holes by needle. After placing the solution for nearly one week, single crystals of **TAHD** were obtained. The same method was used for the preparation of single crystals of **TAND** albeit with different solvent system (methylene chloride: 5 mL, acetonitrile: 1 mL). The single crystal X-ray diffraction data were collected on a Bruker APEX II CCD diffractometer with a graphite monochromatized Mo-K α radiation source (λ = 0.71073 Å). All structures were solved by direct methods and refined by full-matrix least-squares on F2 using the APEX 2 program package. All the nonhydrogen atoms were refined with anisotropic thermal parameters. CCDC number for **TAHD** and **TAND** are 1408693 and 1408694, respectively.

Device's fabrication and characterization

Electrode fabrication

To fabricate the electrodes for photoelectrochemical measurements, ~ 10 mg of the samples (**TAHD** and **TAND**) were added into 2 ml of chloroform. Then the mixtures were subjected to brief sonication in a water bath until the samples were fully dissolved in chloroform. Fluorine-doped tin oxide (FTO) coated glasses ($1.0 \times 2.5 \text{ cm}^2$) were used as the substrate for the electrode fabrication. The substrates were cleaned thoroughly by sonication in 5% detergent (Decon® 90) for 30 minutes first and then rinsed with de-ionized water (DI water) for several times, which were followed by sonication in DI water for 15 minutes. The sonication in DI water process was repeated for three times. Before coating with samples, the FTO substrates were cleaned with UV-ozone plasma for 15 minutes to remove the organic residues. After that, 50 μL of different sample solutions were dropped onto the surface of FTO substrates, which were masked using Ti foil with an effective area of $1.0 \times 1.0 \text{ cm}^2$. The samples were first dried naturally in the dark to avoid the photochemical formation of phosgene, and then placed in a 60°C oven for 30 minutes.

Photoelectrochemical measurements

The photoelectrochemical measurements were carried out in a 22.5 ml extrasil (ES) quartz cell filled with 0.5 M Na_2SO_4 aqueous solution (pH = 7.2), using an electrochemical workstation (CHI 760E). Prior to the measurement, the electrolyte was degassed by purging with argon continuously for 30 minutes. A 300 W xenon lamp (Newport) coupled to an AM 1.5 G filter was used as the standard light source, and the illumination intensity of the surface of the photoelectrode was ~ 100 mW/cm^2 , calibrated using a standard silicon photodiode. Three-electrode set-up, with a platinum plate ($1.0 \times 2.0 \text{ cm}^2$) and a silver-silver chloride (Ag/AgCl , in 3 M KCl) as the counter and reference electrodes, respectively, to study the photovoltage response (illuminated open circuit potential) of the samples. Meanwhile, the photocurrent was carried out using a two-electrode set-up, in which the working electrode and the counter electrode were short-circuited.

Mott-Schottky measurement

The Mott-Schottky plots of different samples were generated using impedance-potential technique. The capacitance of the semiconductor–electrolyte interface was collected at 1kHz, with 10 mV AC voltage amplitude, in the same electrolyte (0.5 M Na_2SO_4 , pH=7.2) and setup for PEC measurements. For estimating the flat-band potential of the samples, the measured voltage was converted into RHE scale by applying the following calculation:

$$V_{\text{RHE}} = V_{\text{measured}} + V_{\text{Ag}/\text{AgCl}}^0 + 0.059 \times \text{pH}$$

Where V_{RHE} is the converted potential, V_{measured} is the potential reading from potentiostat and $V_{\text{Ag}/\text{AgCl}}^0$ is the potential difference between Ag/AgCl reference electrode and standard hydrogen electrode (SHE).

Conclusions

In summary, two N-heteroquinones (**TAHD** and **TAND**) have been successfully synthesized and fully characterized. Studies showed that the length of N-heteroquinones has large effect on the physical properties, crystal packing and photoelectrical behaviors. Further studies will focus on other possible applications in organic electronics especially with the longer N-heteroquinone **TAND**.

Acknowledgements

Q.Z. acknowledges financial support from AcRF Tier 1 (RG 133/14) and Tier 2 (ARC 20/12 and ARC 2/13) from MOE, and the CREATE program (Nanomaterials for Energy and Water Management) from NRF, Singapore. Q.Z. also thanks the support from Open Project of State Key Laboratory of Supramolecular Structure and Materials (Grant number: sklsm2015027), Jilin University, China. J.L, G.L and Y.Z are supported by the Singapore National Research Foundation through the Competitive Research Programme (CRP) under Project No. NRF-CRP5-2009-04. Y.L. thanks the support from the Molecular Foundry, which is supported by the Office of Science, Office of Basic Energy Sciences, of the U.S. Department of Energy under Contract No. DE-AC02-05CH11231.

Notes and references

- (a) U. H. F. Bunz, J. U. Engelhart, B. D. Lindner and M. L. Schaffroth, *Angew. Chem. Int. Ed.*, 2013, **52**, 3810–3821. (b) U. H. F. Bunz, *Chem. Eur. J.*, 2009, **15**, 6780–6789. (c) A. L. Appleton, S. M. Brombosz, S. Barlow, J. S. Sears, J. L. Bredas, S. R. Marder and U. H. F. Bunz, *Nat. Commun.*, 2010, **1**, 91. (d) Q. Miao, *Synlett.*, 2012, **23**, 326–336. (e) G. J. Richards, J. P. Hill, T. Mori and K. Ariga, *Org. Biomol. Chem.*, 2011, **9**, 5005–5017. (f) J. B. Li and Q. C. Zhang, *ACS Appl. Mater. Interfaces*, 2015, 10.1021/acsami.5b00113.
- (a) J. E. Anthony, *Chem. Rev.*, 2006, **106**, 5028–5048. (b) J. E. Anthony, *Angew. Chem. Int. Ed.*, 2008, **47**, 452–483. (c) Z. Sun, Q. Ye, C. Y. Chi and J. S. Wu, *Chem. Soc. Rev.*, 2012, **41**, 7857–7889. (d) J. B. Li and Q. C. Zhang, *Synlett.*, 2013, **24**, 686–696. (e) Q. Ye and C. Y. Chi, *Chem. Mater.*, 2014, **26**, 4046–4056. (f) M. Watanabe, Y. J. Chang, S. W. Liu, T. H. Chao, K. Goto, M. M. Islam, C. H. Yuan, Y. T. Tao, T. Shinmyozu and T. J. Chow, *Nature Chem.*, 2012, **4**, 574–578.
- (a) Q. Miao, *Adv. Mater.*, 2014, **26**, 5541–5549. (b) J. U. Engelhart, B. D. Lindner, M. Schaffroth, D. Schrempp, O. Tverskoy and U. H. F. Bunz, *Chem. Europ. J.*, 2015, **21**, 8121–8129. (c) J. U. Engelhart, B. D. Lindner, O. Tverskoy, F. Rominger and U. H. F. Bunz, *Org. Lett.*, 2012, **14**, 1008–1011. (d) B. D. Lindner, J. U. Engelhart, A. L. Appleton, F. Rominger, A. Peters, H. J. Himmel and U. H. F. Bunz, *Angew. Chem. Int. Ed.*, 2011, **50**, 8588–8591. (e) J. B. Li, F. Yan, J. K. Gao, P. Z. Li, W. W. Xiong, Y. L. Zhao, X. W. Sun and Q. C. Zhang, *Dyes Pigm.*, 2015, **112**, 93–98. (f) J. B. Li, P. Z. Li, J. S. Wu, J. K. Gao, W. W. Xiong, G. D. Zhang, Y. L. Zhao and Q. C. Zhang, *J. Org. Chem.*, 2014, **79**, 4438–4445.
- (a) Z. K. He, D. Q. Liu, R. X. Mao, Q. Tang and Q. Miao, *Org. Lett.*, 2012, **14**, 1050–1053. (b) Q. Miao, T. Q. Nguyen, T. Someya, G. B. Blanchet and C. Nuckolls, *J. Am. Chem. Soc.*, 2003, **125**, 10284–10287. (c) F. Paulus, B. D. Lindner, H. Reiß,

- F. Rominger, A. Leineweber, Y. Vaynzof, H. Sirringhaus and U. H. F. Bunz, *J. Mater. Chem. C*, 2015, **3**, 1604–1609.
- 5 (a) C. L. Song, C. B. Ma, F. Yang, W. J. Zeng, H. L. Zhang and X. Gong, *Org. Lett.*, 2011, **13**, 2880–2883. (b) Y. Y. Liu, C. L. Song, W. J. Zeng, K. G. Zhou, Z. F. Shi, C. B. Ma, F. Yang, H. L. Zhang and X. Gong, *J. Am. Chem. Soc.*, 2010, **132**, 16349–16351.
- 6 Z. X. Liang, Q. Tang, J. B. Xu and Q. Miao, *Adv. Mater.*, 2011, **23**, 1535–1539.
- 7 (a) P. Biegger, S. Stolz, S. N. Intorp, Y. X. Zhang, J. U. Engelhart, F. Rominger, K. I. Hardcastle, U. Lemmer, X. H. Qian, M. Hamburger and U. H. F. Bunz, *J. Org. Chem.*, 2015, **80**, 582–589. (b) B. D. Lindner, Y. X. Zhang, S. Höfle, N. Berger, C. Teusch, M. Jesper, K. I. Hardcastle, X. H. Qian, U. Lemmer, A. Colsmann, U. H. F. Bunz and M. Hamburger, *J. Mater. Chem. C*, 2013, **1**, 2718–5724. (c) G. Li, A. P. Abiyasa, J. K. Gao, Y. Divayana, W. Q. Chen, Y. Zhao, X. W. Sun and Q. C. Zhang, *Asian J. Org. Chem.*, 2012, **1**, 346–351.
- 8 Y. C. Wu, Z. Y. Yin, J. C. Xiao, Y. Liu, F. X. Wei, K. J. Tan, C. Kloc, L. Huang, Q. Y. Yan, F. Z. Hu, H. Zhang and Q. C. Zhang, *ACS Appl. Mater. Interfaces*, 2012, **4**, 1883–1886.
- 9 Q. C. Zhang, J. C. Xiao, Z. Y. Yin, H. M. Duong, F. Qiao, Y. C. Freddy Boey, X. Hu, H. Zhang and Wudl, *F. Chem. Asian. J.*, 2011, **6**, 856–862.
- 10 G. Li, J. W. Miao, J. Cao, J. Zhu, B. Liu and Q. C. Zhang, *Chem. Commun.*, 2014, **50**, 7656–7658.
- 11 (a) G. Li, K. Zheng, C. Y. Wang, K. S. Leck, F. Z. Hu, X. W. Sun and Q. C. Zhang, *ACS Appl. Mater. Interfaces*, 2013, **5**, 6458–6462. (b) P. Y. Gu, F. Zhou, J. K. Gao, G. Li, C. Y. Wang, Q. F. Xu, Q. C. Zhang and J. M. Lu, *J. Am. Chem. Soc.*, 2013, **135**, 14086–14089. (c) C. Y. Wang, B. L. Hu, J. X. Wang, J. K. Gao, G. Li, W. W. Xiong, B. H. Zou, M. Sunzuki, N. Aratani, H. Yamada, F. W. Huo, P. S. Lee and Q. C. Zhang, *Chem. Asian. J.*, 2015, **10**, 116–119. (d) C. Y. Wang, J. X. Wang, P. Z. Li, J. K. Gao, S. Y. Tan, W. W. Xiong, B. L. Hu, P. S. Lee, Y. L. Zhao and Q. C. Zhang, *Chem. Asian. J.*, 2014, **9**, 779–783. (e) P. Y. Gu, J. K. Gao, C. J. Lu, W. Q. Chen, C. Y. Wang, G. Li, F. Zhou, Q. F. Xu, J. M. Lu and Q. C. Zhang, *Mater. Horiz.* 2014, **1**, 446–451.
- 12 (a) J. B. Li, J. K. Gao, G. Li, W. W. Xiong and Q. C. Zhang, *J. Org. Chem.*, 2013, **78**, 12760–12768. (b) J. J. Bryant, Y. X. Zhang, B. D. Lindner, E. A. Davey, A. L. Appleton, X. H. Qian and U. H. F. Bunz, *J. Org. Chem.*, 2012, **77**, 7479–7486. (c) J. B. Li, J. K. Gao, W. W. Xiong, P. Z. Li, H. C. Zhang, Y. L. Zhao and Q. C. Zhang, *Chem. Asian. J.*, 2014, **9**, 121–125. (d) J. F. Zhao, G. Li, C. Y. Wang, W. Q. Chen, S. C. J. Loo and Q. C. Zhang, *RSC Adv.*, 2013, **3**, 9653–9657. (e) G. Li, J. K. Gao and Q. C. Zhang, *Asian J. Org. Chem.*, 2014, **3**, 203–208.
- 13 (a) J. U. Engelhart, O. Tverskoy and U. H. F. Bunz, *J. Am. Chem. Soc.*, 2014, **136**, 15166–15169. (b) J. K. Gao and Q. C. Zhang, *Israel J. Chem.* 2014, **5**, 699–702. (c) U. H. F. Bunz, *Acc. Chem. Res.*, 2015, DOI: 10.1021/acs.accounts.5b00118.
- 14 (a) J. A. VanAllan, G. A. Reynolds and R. E. Adel, *J. Org. Chem.*, 1963, **15**, 3965–3969. (b) G. M. Badger and R. Pettim, *J. Chem. Soc.*, 1951, 3211–3215. (c) M. A. Fox and T. A. Voynick, *J. Org. Chem.*, 1981, **46**, 1235–1239.
- 15 (a) Q. Tang, Z. X. Liang, J. Liu, J. B. Xu and Q. Miao, *Chem. Commun.*, 2010, **46**, 2977–2979. (b) Z. X. Liang, Q. Tang, J. Liu, J. H. Li, F. Yan and Q. Miao, *Chem. Mater.*, 2010, **22**, 6438–6443.
- 16 (a) S. B. Miao, A. L. Appleton, N. Berger, S. Barlow, S. R. Marder, K. I. Hardcastle, U. H. F. Bunz, *Chem. Eur. J.*, 2009, **15**, 4990–4993. (b) O. Tverskoy, F. Rominger, A. Peters, H. J. Himmel and U. H. F. Bunz, *Angew. Chem. Int. Ed.*, 2011, **50**, 3557–3560.
- 17 C. Y. Wang, J. Zhang, G. K. Long, N. Aratani, H. Yamada, Y. Zhao and Q. C. Zhang, *Angew. Chem. Int. Ed.*, 2015, **54**, 6292–6296.
- 18 (a) A. C. Kozytskiy, O. L. Stroyuk and S. Y. Kuchimiy, *Catal. Today*, 2014, **230**, 227–233. (b) X. Y. Yang, A. Wolcott, G. M. Wang, A. Sobo, R. C. Fitzmorris, F. Qian, J. Z. Zhang and Y. Li, *Nano Lett.*, 2009, **9**, 2331–2336.
- 19 S. B. Miao, S. M. Brombosz, P. V. R. Schleyer, J. I. Wu, S. Barlow, S. R. Marder, K. I. Hardcastle and U. H. F. Bunz, *J. Am. Chem. Soc.*, 2008, **130**, 7339–7344.
- 20 A. L. Appleton, S. B. Miao, S. M. Brombosz, N. J. Berger, S. Barlow, S. R. Marder, B. M. Lawrence, K. I. Hardcastle and U. H. F. Bunz, *Org. Lett.*, 2009, **11**, 5222–5225.
- 21 A. L. Appleton, S. Barlow, S. R. Marder, K. I. Hardcastle and U. H. F. Bunz, *Synlett.*, 2011, **14**, 1983–1986.
- 22 (a) A. D. Becke, *J. Chem. Phys.*, 1993, **98**, 5648–5652. (b) C. Lee, W. Yang, R. G. Parr, *Phys. Rev. B* 1988, **37**, 785–789.
- 23 J. B. Li, Y. B. Zhao, J. Lu, G. Li, J. P. Zhang, Y. Zhao, X. W. Sun and Q. C. Zhang, *J. Org. Chem.*, 2015, **80**, 109–113.